Atmos. Chem. Phys. Discuss., 14, 1617–1645, 2014
www.atmos-chem-phys-discuss.net/14/1617/2014/
doi:10.5194/acpd-14-1617-2014

Atmospheric Chemistry and Physics Discussions

Influence of cloud processing on CCN activation behaviour in the Thuringian Forest, Germany during HCCT-2010

S. Henning[1], K. Dieckmann[1], K. Ignatius[1], M. Schäfer[1,*], P. Zedler[1], E. Harris[2,], B. Sinha[2,3], D. van Pinxteren[1], S. Mertes[1], W. Birmili[1], M. Merkel[1], Z. Wu[1], A. Wiedensohler[1], H. Wex[1], H. Herrmann[1], and F. Stratmann[1]**

[1]Leibniz Institute for Tropospheric Research, 04318 Leipzig, Germany
[2]Particle Chemistry Department, Max Planck Institute for Chemistry, Hahn-Meitner-Weg 1, 55128 Mainz, Germany
[3]Department of Earth Sciences, IISER Mohali, Sector 81, SAS Nagar, Manauli PO 140306, India
[*]now at: University of Leipzig, Faculty of Physics and Earth Sciences Leipzig Institute for Meteorology (LIM), Stephanstr. 3, 04103 Leipzig, Germany
[**]now at: Laboratory for Air Pollution and Environmental Technology, Swiss Federal Institute for Materials Science and Technology (EMPA), Überlandstrasse 128, 8600 Dübendorf, Switzerland

Received: 19 December 2013 – Accepted: 7 January 2014 – Published: 17 January 2014

Correspondence to: S. Henning (henning@tropos.de)

Published by Copernicus Publications on behalf of the European Geosciences Union.

ACPD
14, 1617–1645, 2014

Abstract

Within the framework of the international cloud experiment “Hill Cap Cloud Thuringia 2010” (HCCT-2010), the influence of cloud processing on the activation properties of ambient aerosol particles was investigated. Particles were probed up- and downwind of an orographic cap cloud on Mt. Schmücke, which is part of a large mountain ridge in Thuringia, Germany. The activation properties of the particles were investigated by means of size-segregated Cloud Condensation Nuclei (CCN) measurements at 3 to 4 different supersaturations. The observed CCN spectra together with the total particle spectra were used to calculate the hygroscopicity parameter κ for the up- and the downwind stations. The up- and downwind critical diameters and κ values were then compared for defined Cloud Events and Non Cloud Events. Cloud processing was found to significantly increase the hygroscopicity of the aerosol particles, with an average increase in κ of 50 %. Mass spectrometry analysis and isotopic analysis of the particles show that the observed increase in hygroscopicity of the cloud-processed particles is due to an enrichment of nitrate and sulfate in the particle phase.

1 Introduction

Clouds are a key parameter in climate change prediction, due to their strong impact on the radiation processes in the atmosphere. However, the effect of aerosol particles on cloud formation, cloud glaciation and precipitation is still insufficiently quantified and remains therefore one of the largest uncertainties in climate change predictions (Lohmann and Feichter, 2005; IPCC, 2013). Studying the interaction of aerosol and clouds under natural conditions is challenging due to the height as well as the spatial and temporal variability of clouds. Aside from extensive airplane, balloon or helicopter investigations of natural clouds (e.g., Krämer et al., 2013, p. 337), a well-established method for cloud investigation is to take advantage of natural clouds reaching the ground, allowing for ground-based experiments. This experimental design allows e.g

ACPD
14, 1617–1645, 2014

the investigation of fog formation (e.g. Po valley fog experiments, Svenningsson et al., 1992), advected stratiform clouds (e.g. Kleiner Feldberg, Wobrock et al., 1994) and also orographically triggered clouds (e.g. Schmücke, Herrmann et al., 2005).

One variation of the ground-based cloud experiments is a Lagrangian-type design. This involves locating several measurement stations in the predominant flow directions above a ridge, in order to probe the air masses before, during and after cloud passage (e.g., Bower et al., 1999; Herrmann et al., 2005). The use of hill cap clouds as a natural flow-through reactor was for example successfully realized on Great Dun Fell (UK) (Bower et al., 1999; Choularton et al., 1997; Svenningsson et al., 1997), on the German mountain Kleiner Feldberg (Wobrock et al., 1994), during the ACE-2 HILLCLOUD experiment at Teneriffe, Spain (Bower et al., 2000) and during FEBUKO at Mt. Schmücke (Herrmann et al., 2005).

The findings here presented, were observed during the cloud experiment "Hill Cap Cloud Thuringia 2010" (HCCT-2010), which was also conducted at the low mountain ridge around Mt. Schmücke, where FEBUKO (Herrmann et al., 2005) took place. HCCT-2010 took place in September/October 2010 and dealt with several aspects of cloud microphysics and chemistry. An overview of HCCT-2010 is given in a companion paper in this special issue.

During the previous FEBUKO campaign, particle number size distribution measurements upwind (ambient) and on the summit (in-cloud: interstitial and residuals) were used to investigate the dependence of the scavenged aerosol fraction on the soluble volume fraction of the observed particles (Mertes et al., 2005a). In addition, at the upwind site the hygroscopic properties were investigated (Lehmann et al., 2005) using Hygroscopic Tandem Differential Mobility Analyzer (HTDMA) measurements. Promising results were achieved concerning the dependence of the scavenged aerosol fraction on the soluble volume fraction of the particles were achieved. However, directly comparable activation or hygroscopicity measurements before and after the cloud passage were not carried out during FEBUKO. Aerosol processing was investigated by model simulation (Tilgner et al., 2005) and by comparing number size distribution up-

ACPD
14, 1617–1645, 2014

wind and downwind (Mertes et al., 2005b). Both studies show an effect on the aerosol size distribution in the size range of the activation diameter and an increase in aerosol number and mass.

The focus of the work presented here was to investigate the influence of cloud processing on the activation properties of aerosol particles. The interaction of particles with water can be theoretically described via Köhler theory (Köhler, 1936), which gives the equilibrium vapor pressure over an aqueous solution droplet. The maximum of the Köhler curve gives the critical supersaturation necessary for droplet activation. Classical Köhler theory needs several input parameters (e.g., molar weight of the particle substance, surface tension of mixture) which are usually unknown for atmospheric particles. Therefore, one-parameter approximations were developed (e.g., Petters and Kreidenweis, 2007; Wex et al., 2007) which are applicable for the description of particle hygroscopic growth as well activation properties. One-parameter approaches are also well suited as a simple measure to implement particles' activation behaviour in modeling studies (e.g., Pringle et al., 2009).

The results presented in this study are based on size-segregated CCN measurements at the up- and downwind station during periods of connected flow. The hygroscopicity parameter κ was deduced from the derived activation diameters. For selected non-precipitating cloud events on Mt. Schmücke the droplet activation properties at the upwind and downwind valley station were compared, and the statistical significance of the findings was tested, in order to measure the influence of cloud passage on particle hygroscopicity. The same comparison between up- and downwind station was also done for defined cloud-free periods as a control experiment.

2 Experimental design and setup

The experiments were conducted as part of the HCCT-2010 campaign, a Lagrangian-style experiment in which air parcels were probed at several locations during passage through an orographic cloud, focussing on the influence of cloud presence on the phys-

ACPD
14, 1617–1645, 2014

ical and chemical properties of the air parcel of interest (see companion paper for details). Briefly, measurements of meteorological parameters and physical and chemical aerosol and gas properties were conducted at three sites along the mountain ridge of the Thuringian forrest, Germany: one upwind station, the in-cloud mountain peak station on Mt. Schmücke and one downwind station (Fig. 1).

Time periods with optimal connected flow between the three stations were chosen by applying several different methods, e.g. shape of particle number size distribution, wind direction, wind speed and ozone concentration (Tilgner et al., 2014). These connected flow regimes were subdivided into periods with a cap cloud present on Mt. Schmücke and the valley sites cloud free, so-called Full Cloud Events (FCE, cf. Table 1), and cloud-free periods at all three stations, called Non Cloud Events (NCE). The FCE and NCE events with CCN measurements available at Goldlauter and Gehlberg station are listed in Table 1 together with liquid water content (LWC), wind direction (wd) and wind speed (ws) on Mt. Schmücke. By coincidence, the FCE time periods with CCN data available at both valley stations had an approaching flow from south-western direction while for the NCE cases the flow was approaching from north-eastern direction. This was taken into account in the data analysis and does not significantly affect the findings.

2.1 Measurement sites

The size-segregated CCN measurements took place at the up- and downwind sites either side of Mt. Schmücke, Gehlberg (GB) and Goldlauter (GL).

The valley station Goldlauter (GL, 50°38′14″ N, 10°45′13″ E), is situated on the southwestern slope of the Thuringian forest mountain ridge. For FCE (southwest wind) this was the upwind station, i.e. the air parcel was probed here before entering the cap cloud and therefore represents the "pre-cloud" status of the aerosol. For NE_NCE (northeast wind) Goldlauter was the downwind station. All measurement equipment was placed inside an air-conditioned container. On top of the container a PM_{10} inlet followed by a self-regenerating diffusion drier was placed (Tuch et al., 2009), maintaining the relative humidity of the aerosol flow below 20 %. Inside the container – beside other

ACPD
14, 1617–1645, 2014

instrumentation – a Mobility Particle Size Spectrometer (MPSS-type TROPOS; details of this instrument in Wiedensohler et al., 2012) was used to determine the particle number size distributions between 10 and 850 nm, and a Cloud Condensation Nucleus counter (CCNc, CCN-100, DMT Boulder, Roberts and Nenes, 2005) in combination with a Differential Mobility Analyser (DMA) was used to measure CCN distributions between 25 and 300 nm.

The measurement equipment at the FCE downwind station Gehlberg (GB, 50°40′21″ N, 10°47′34″ E) was also placed inside an air conditioned container. Here the PM_{10} inlet was followed by individual drier systems in front of the instruments instead of the self-regenerating diffusion drier applied in GL. This was the only difference in the size-segregated CCN measurement set-up between both stations. Nafion driers (30 cm, TROPOS-custom-made) have been placed in front of the another TROPOS-type mobility particle size spectrometer and the DMA-CCNc, both of which kept the RH stable below 20 %. The data were corrected for the individual particle losses due to tubing and driers.

At these two sites and at Mt. Schmücke (SM, 50°39′17″ N, 10°46′30″ E, 916 m a.s.l.) size-resolved (coarse and fine) particulate matter was collected for sulfur isotope analysis, with the in-cloud particulate separated into cloud droplet residual and interstitial fractions. In addition, at the upwind and downwind stations, SO_2 and H_2SO_4 gas and ultrafine particulate matter were collected. Combined scanning electron microscopy (SEM) and NanoSIMS measurements were used to determine the $\delta^{34}S$ values of the samples, with particulate isotopic measurements resolved for particle type (Harris et al., 2013, 2014).

2.2 Size-segregated CCN measurements

The set-up for the size segregated activation measurements was identical at the up- and downwind stations (Fig. 2), apart from the different drier types (cf. above). Downstream of the aerosol inlet and the drier unit, the 1 L min^{-1} aerosol flow passed through a neutralizer to achieve the bipolar charge equilibrium (Wiedensohler, 1988).

ACPD
14, 1617–1645, 2014

The DMAs ran with an aerosol to sheath air flow of 1/10 to size-select aerosol particles based on electrical mobility, to achieve a quasi-monodisperse aerosol distribution. Multiply-charged particles with larger sizes were also selected, for which the size and activation scans had to be corrected, using the bipolar charge distribution. Downstream of the DMA a flow of 0.5 L min^{-1} particle-free air was added to the aerosol flow and the total flow was divided between to a particle counter (1 L min^{-1} working flow, CPC 3010, TSI Aachen Germany) and a cloud condensation nucleus counter (0.5 L min^{-1} working flow, CCNc, CCN-100, Boulder, USA). Measurements at Goldlauter station were taken from 11 September 2010 to 20 October 2010 and in Gehlberg from 12 September 2010 to 20 October 2010, which is slightly shorter than the duration of the whole HCCT-2010 campaign.

The CCNc, a stream-wise thermal gradient cloud condensation nucleus counter (Roberts and Nenes, 2005), was applied to investigate supersaturation-dependent activation of the particles. In this instrument the inlet flow is split into a particle-free sheath air flow, which is kept particle-free via a filter, and an aerosol flow. The sheath air is humidified before entering the flow tube and surrounds the aerosol at the centerline. The stream-wise temperature gradient applied in the flow tube determines the supersaturation to which the particles are exposed. The number of activated particles (N_{CCN}) is detected at the end of the flow tube with an optical counter. The ratio between the CCN number and the total particle number (N) gives the activated fraction (AF) of the particles. The CCNc is either used to measure saturations scans, meaning that the particle diameter is kept constant and the saturation is varied, or to measure diameter scans for which the saturation is fixed and the diameter is varied. A saturation scan is used to determine the critical supersaturation, which by definition is the saturation at which 50 % of the particles of a particular size are activated (AF = 0.5). The critical diameter D_c, the diameter at which 50 % of the particles are activated at a particular supersaturation, is derived from a diameter scan. In this study we ran diameter scans for four fixed supersaturations (0.07, 0.1, 0.2, 0.4 %).

ACPD
14, 1617–1645, 2014

The supersaturation reached in the CCNc during the size-segregated CCN measurements was calibrated with ammonium sulfate particles. This was done by atomizing an ammonium sulfate-water solution ($0.1\,\mathrm{g}\,(NH_4)_2SO_4\,(300\,\mathrm{mL}\,H_2O)^{-1}$), passing the resulting aerosol through a diffusion dryer, and injecting the dried particles into the CCN measurement set-up (Fig. 2). The calibration procedure followed that described in Rose et al. (2008). In short, diameter scans were run at nominal supersaturations between 0.07 and 0.7 %, which relate to a certain temperature gradient in the flow tube of the CCNc. The AF were fitted applying a Gaussian error function to the data:

$$\mathrm{AF} = \frac{a+b}{2}\left[1+\mathrm{erf}\left(\frac{D-D_\mathrm{c}}{\sigma\sqrt{2}}\right)\right], \quad (1)$$

where a and b are the upper and lower limit, to calculate critical diameters D_c at the set nominal supersaturations. As $(NH_4)_2SO_4$ particles were used, the activation diameter is known and the set temperature gradient in the instrument can be related to the effective supersaturation SS reached in the column. Repeated calibrations show an achievable accuracy in SS of 10 % (relative) at supersaturations above SS = 0.2 % and $\delta\mathrm{SS} \leq 0.02$ % (absolute) at lower supersaturations (Gysel and Stratmann, 2013).

In the work presented here, we apply the single parameter κ Köhler theory (Petters and Kreidenweis, 2007) to describe the hygroscopicity of the ambient particles. The hygroscopicity parameter κ is calculated in the following way (from Petters and Kreidenweis, 2007):

$$\kappa = \frac{4A^3}{27D_\mathrm{c}^3\ln^2\mathrm{SS}}, \quad (2)$$

with

$$A = \frac{4\sigma_{s/a}M_\mathrm{w}}{RT\rho_\mathrm{w}}. \quad (3)$$

ACPD
14, 1617–1645, 2014

The critical diameter is determined by fitting the AF scans to the error function (Eq. 1), analogously to the calibration procedure. The calibrated SS and measured D_c are inserted into into Eq. (2) to calculate κ at fixed supersaturations for ambient particles. The error in SS setpoint, especially at low supersaturations, results in quite a large level of uncertainty in κ values. A critical diameter D_c of e.g. 200 nm at a SS of 0.07 % ± 0.02 % corresponds to a κ range from 0.21 (SS = 0.09 %) < 0.35 < 0.94 (SS = 0.05 %). This is a critical point in working with κ and has to be considered in the interpretation. This will be discussed more in Sect. 3.2.

2.3 Particle number size distribution measurements

In parallel to the CCN spectra, the particle number size distribution in the size range between 10 and 850 nm have been measured in Goldlauter and Gehlberg. The measurements were done with the above mentioned mobility particle size spectrometers, which were connected to the same PM_{10} inlet as described above for the CCN measurements. Particle losses due to diffusion in the instrument and in the sampling lines have been corrected according to the method of "equivalent length" as described in Wiedensohler et al. (2012).

The CCN spectra have to be corrected for multiply-charged particles as the fitting of the AF with the error function is influenced by the appearance of a second step in the CCN spectra (Rose et al., 2008). This step is triggered by the fact that multiply-charged large particles have the same electrical mobility diameter as singly-charged smaller particles, and are thus falsely selected in the DMA. In the CCNc, however, they activate at a lower supersaturation than the singly-charged particles, and appear in the activated fraction vs. particle diameter curve as a first activation step at smaller diameters. How pronounced this first step is depends on the particle number size distribution, especially on the number of larger particles. The correction is described in detail in Deng et al. (2011): in brief, starting at larger sizes the number of possible multiply-charged particles at one size is calculated based on the charge equilibrium (Wiedensohler, 1988) and subtracted from the particle number at the corresponding

ACPD
14, 1617–1645, 2014

smaller sizes. This is done for the whole N and N_{CCN} distribution from large to small particles.

3 Results and discussion

Ideally, a fixed time difference of 20 min would applied to compare upwind and downwind measurements, i.e. the measurement from the upwind station would be paired with a measurement from the downwind station, which was taken 20 min later. However, the set supersaturation should be the same at both stations for comparable measurements. Therefore, downwind data within 60 min of the upwind time stamp was included in the analysis. The number of activation measurements (n) per supersaturation (SS) for the matching time periods are given in Table 2.

3.1 Activation diameter and hygroscopicity parameter κ

The averaged values of the critical diameter (D_c), its standard deviation (σD_c) and the hygroscopicity parameter κ for each SS across all Full Cloud Events (FCE) and Non Cloud Events (NCE) are given in Table 2. We merged all the FCE data and respectively all the NCE data to have a better statistical basis. During cloud events, D_c at the upwind station was observed to be larger than at the downwind station, with upwind values between 194.3 (SS = 0.07 %) and 122.9 nm (SS = 0.2 %) compared to downwind D_c between 173.9 (SS = 0.07 %) and 101.5 nm (SS = 0.2 %). Consequently, during cloud events, the calculated κ values at the upwind station (0.4, 0.42 and 0.20 for SS of 0.07, 0.1 and 0.2 %) were smaller than after cloud passage, where κ values of 0.54, 0.54 and 0.32 at SS of 0.07, 0.1 and 0.2 % were calculated. No significant change in D_c and κ was observed for non-cloud events ($n = 55$, $p > 0.01$).

In Fig. 3a and b the results are illustrated. The error bars were calculated by assuming a maximum absolute error in SS of ±0.02 % for SS ≤ 0.2 % and assuming a 10 % relative uncertainty for SS > 0.2 % (Gysel and Stratmann, 2013), and applying Eq. (2)

ACPD
14, 1617–1645, 2014

to calculate κ. Due to the asymmetric relation between SS and κ also the error bars are asymmetric and give the maximum uncertainty in κ. The increase in κ after the cloud passage in the FCE is obvious, whereas in the NCE the data fall together on the 1 : 1 line. However, the observed effect is within the measurement uncertainty – especially for the lower supersaturations. Therefore, we tested the statistical significance of the change in critical diameters (and thus κ values) between the stations during FCE and NCE, and re-estimated the uncertainty of κ by modeling the instrumental error in supersaturation.

3.2 Statistical analysis of the critical diameters and κ uncertainty estimation

We used statistical testing to determine if the change from upwind critical diameters $D_{c,up}$ to downwind critical diameters $D_{c,down}$ is significantly different between cloud and non-cloud events. This statistical testing scheme is known as "between-within" or "mixed" design, and it is analogous to the statistical experimental design in medicine called the "pre-post case control study" in which half of the patients are given medicine and the other half placebo, and the patients are tested before and after the treatment. The experimental design is illustrated in Fig. 4. While testing, it is essential to take into account that the pre- and post- (up- and downwind) measurement points during the same day are paired, which accounts for variability between days and thus reduces noise. The simplest statistical test for a mixed design is called Change Score Analysis (Oakes and Feldman, 2001), which is essentially a t test between Δ_{FCE} and Δ_{NCE} where $\Delta = D_{c,up} - D_{c,down}$. The null hypothesis was that there is no difference between FCE and NCE for $D_{c,down}$ with respect to $D_{c,up}$. A confidence of $p < 0.01$ was needed to reject the null hypothesis. The statistical analysis showed that for every supersaturation (0.07 %, 0.1 %, 0.2 %) the downwind critical diameters with respect to upwind diameters were significantly smaller during FCE than during NCE, with p values of 2.676×10^{-5}, 1.404×10^{-3} and 3.137×10^{-5} for 0.07 %, 0.1 % and 0.2 % supersaturations, respectively. The critical diameter data sets for each supersaturation were tested

ACPD
14, 1617–1645, 2014

separately. 0.4 % supersaturation was excluded from testing because there was no data for FCE periods.

We also checked with a t test that there is no significant difference between the FCE and NCE upwind critical diameters, to show that the differences in downwind critical diameters are caused by the cloud processes. As statisticians disagree on the correct statistical tests for mixed designs (Senn, 2006), we applied also the Analysis of Covariance (ANCOVA), assuming a linear model $D_{c,down} = \alpha + \text{cloudiness} + D_{c,up} + \epsilon$, where α is an intercept term, cloudiness is the parameter defining if the data point was measured during an FCE or NCE day and ϵ is a Gaussian noise term. This test is used to investigate the statistical significance of the term cloudiness, using $D_{c,up}$ values as covariates. The results given by ANCOVA (not shown) are in good agreement with the p values obtained from the Change Score Analysis.

Next, we estimated the uncertainty distribution of κ with Monte Carlo simulations. The instrumental supersaturation error of the CCNc is Gaussian, with standard deviations of 0.00714 for 0.07 %, 0.1 % and 0.2 % supersaturations and 0.01429 for 0.4 % supersaturation. However, due to the nonlinear relationship between κ and the critical diameter, the uncertainty distribution of κ is non-Gaussian. The distribution of κ is simulated for each data point separately by drawing 100 000 random samples from a Gaussian supersaturation distribution ($\mu = 0.07, \sigma = 0.00714$) and using Eq. (2). An example of a simulated κ distribution is presented in Fig. 5, showing the 2.5, 25, 50, 75, 97.5 and 100th percentiles. All the analyses were done using R statistical software (R version 2.15.3, 2013).

By applying this statistical approach to the data, it is possible to present more reasonable error bars, since the original error bars do not give any information about the uncertainty distribution of κ. Figure 6a gives single κ values at the upwind station compared to the κ at the downwind station during FCE. The error bars presented in the figure are the 95 %-confidence interval calculated from Monte Carlo simulations as explained above. All κ values derived for the downwind station are higher than those at the upwind station. The same analysis was again done for the NCE periods (Fig. 6b).

ACPD
14, 1617–1645, 2014

Here, within error bars, the data of all SS fall onto the 1 : 1 line. This leads to the conclusion, that we measured particles in NCE periods with the same hygroscopic properties at both up- and downwind stations. The statistical test results support this conclusion. There is still considerable error in the κ values, however the rigorous statistical analysis showed that the decrease in critical diameters due to cloud processing is significant. The results clearly demonstrate that the particle properties changed between up- and downwind stations only when a hill cap cloud was present, leading to more hygroscopic aerosol particles downwind of the cloud.

3.3 Chemical in-cloud processing of the particles

Our findings can be explained by the enrichment of hygroscopic material in the particles during cloud presence. Assuming a chemical composition similar to the one given in Wu et al. (2013) for the upwind station, with a mass fraction of 40 % organic material and 30 % each of ammonium nitrate and ammonium sulfate we can model the observed κ of e.g. 0.40 (compare Table 2). The measured increase in κ would during FCE translate to an increase in the mass fraction of 20 % in ammonium nitrate and ammonium sulfate between the upwind and downwind stations. This estimate is supported by measurements results from other groups during HCCT-2010, who focussed on the chemical and isotopic signature of the particle population.

Sulfur isotope analysis of the particulate material was used to investigate the in-cloud production of sulfate. Combined gas phase and single particle measurements allowed the dominating sulfate production sources to be identified (Harris et al., 2014). Direct sulfate uptake, through dissolution of H_2SO_4 gas and scavenging of ultrafine particulate, was found to be the most important source for in-cloud addition of sulfate to mixed particles (the most common particle type at HCCT-2010), while in-cloud aqueous oxidation of SO_2 primarily catalyzed by transition metal ions (Harris et al., 2013) was most important for coarse mineral dust.

Consistent with our results of increased hygroscopicity, both offline (impactor) and online (AMS) measurements of the chemical aerosol composition during HCCT often

ACPD
14, 1617–1645, 2014

indicate an increased mass fraction of sulfate in aerosol particles after their passage through a cloud (van Pinxteren, Poulain, D'Anna, personal communications, 2013, data yet to be published in forthcoming companion papers of this special issue).

Mass spectrometric analysis of cloud residuals at the in-cloud station Schmücke showed an enhancement of nitrate in the cloud residuals compared to particles sampled under cloud-free conditions (Schneider et al., 2014). Additionally, a change of mixing state was observed by single particle mass spectrometry (Roth et al., 2014). The cloud residuals showed a higher fraction of particles internally mixed with sulfate and nitrate compared to the particles sampled under cloud free conditions. These findings can be explained by uptake of HNO_3 and sulfate production in the cloud droplets, resulting in an increased hygroscopicity after the cloud passage.

4 Summary and conclusions

In the ground-based cloud experiment HCCT-2010 the activation diameter of aerosol particles were determined before and after passage across a hill. For cases, with a proved connected flow the activation properties of aerosol particle at the up- and downwind stations were compared. For cases with a cap cloud on Mt. Schmücke a decrease in the critical diameter and a consequent increase of about 50 % in the hygroscopicity parameter κ was observed. In the cases with a connected flow between the valley stations and no cloud on the hill top, no change in activation diameter was detected. The statistical significance of these findings was rigorously tested. All the κ values during cloud events were larger at the downwind than upwind station, and the critical diameters were significantly smaller than during non-cloud days. Therefore, we conclude that in-cloud processes significantly increased CCN activity during all observed cloud events at HCCT-2010.

A possible explanation for the increased κ is the enrichment of more hygroscopic material during cloud processing, such as nitrate and sulfate. Particulate isotope measurements support our observations: dissolution of H_2SO_4 and scavenging of ultrafine

ACPD
14, 1617–1645, 2014

particulate in the cloud were identified as being the most important in-cloud sulfate addition process for modifying CCN activity in the majority of particles. Mass spectrometric measurements also corroborate the enrichment of soluble material in the particles during cloud: increased nitrate and a change of mixing state was found in cloud residuals. Our measurements suggest that after cloud dissipation the added hygroscopic material remains in the cloud residual aerosol particles.

Our results demonstrate the strong impact of in-cloud processing on the hygroscopic properties of potential CCN. Consideration of our findings in modeling studies will improve cloud representation substantially.

Acknowledgements. We would like to thank Ilkka Huopaniemi for his advice concerning the statistical approach. The HCCT-2010 campaign was partially funded by the Deutsche Forschungsgemeinschaft (HE 3086/15-1). Stephan Mertes participation was funded by DFG grant ME 3534/1-2.

References

Birmili, W., Stratmann, F., and Wiedensohler, A.: Design of a DMA-based size spectrometer for a large particle size range and stable operation, J. Aerosol Sci., 30, 549–553, 1999.

Bower, B. K. N., Choularton, T. W., Gallagher, M. W., Beswick, K. M., Flynn, M. J., Allen, A. G., Davison, B. M., James, J. D., Robertson, L., Harrison, R. M., Hewitt, C. N., Cape, J. N., McFadyen, G. G., Milford, C., Sutton, M. A., Martinsson, B. G., Frank, G., Swietlicki, E., Zhou, J., Berg, O. H., Mentes, B., Papaspiropoulos, G., Hansson, H. C., Leck, C., Kulmala, M., Aalto, P., Vakeva, M., Berner, A., Bizjak, M., Fuzzi, S., Laj, P., Facchini, M. C., Orsi, G., Ricci, L., Nielsen, M., Allan, B. J., Coe, H., McFiggans, G., Plane, J. M. C., Collett, J. L., Moore, K. F., and Sherman, D. E.: ACE-2 HILLCLOUD: an overview of the ACE-2 ground-based cloud experiment, Tellus B, 52, 750–778, 2000. 1620

Bower, K. N., Choularton, T. W., Gallagher, M. W., Colvile, R. N., Beswick, K. M., Inglis, D. W. F., Bradbury, C., Martinsson, B. G., Swietlicki, E., Berg, O. H., Cederfelt, S. I., Frank, G., Zhou, J., Cape, J. N., Sutton, M. A., McFadyen, G. G., Milford, C., Birmili, W., Yuskiewicz, B. A., Wiedensohler, A., Stratmann, F., Wendisch, M., Berner, A., Ctyroky, P., Galambos, Z., Mes-

ACPD
14, 1617–1645, 2014

fin, S. H., Dusek, U., Dore, C. J., Lee, D. S., Pepler, S. A., Bizjak, M., and Divjak, B.: The Great Dun Fell experiment 1995: an overview, Atmos. Res., 50, 151–184, 1999. 1620

Choularton, T. W., Colvile, R. N., Bower, K. N., Gallagher, M. W., Wells, M., Beswick, K. M., Arends, B. G., Mols, J. J., Kos, G. P. A., Fuzzi, S., Lind, J. A., Orsi, G., Facchini, M. C., Laj, P., Gieray, R., Wieser, P., Engelhardt, T., Berner, A., Kruisz, C., Moller, D., Acker, K., Wieprecht, W., Luttke, J., Levsen, K., Bizjak, M., Hansson, H. C., Cederfelt, S. I., Frank, G., Mentes, B., Martinsson, B., Orsini, D., Svenningsson, B., Swietlicki, E., Wiedensohler, A., Noone, K. J., Pahl, S., Winkler, P., Seyffer, E., Helas, G., Jaeschke, W., Georgii, H. W., Wobrock, W., Preiss, M., Maser, R., Schell, D., Dollard, G., Jones, B., Davies, T., Sedlak, D. L., David, M. M., Wendisch, M., Cape, J. N., Hargreaves, K. J., Sutton, M. A., StoretonWest, R. L., Fowler, D., Hallberg, A., Harrison, R. M., and Peak, J. D.: The Great Dun Fell cloud experiment 1993: an overview, Atmos. Environ., 31, 2393–2405, doi:10.1016/s1352-2310(96)00316-0, 1997. 1620

DeCarlo, P. F., Kimmel, J. R., Trimborn, A., Northway, M. J., Jayne, J. T., Aiken, A. C., Gonin, M., Fuhrer, K., Horvath, T., Docherty, K. S., Worsnop, D. R., and Jimenez, J. L.: Field-deployable, high-resolution, time-of-flight aerosol mass spectrometer, Anal. Chem., 78, 8281–8289, doi:10.1021/ac061249n, 2006.

Deng, Z. Z., Zhao, C. S., Ma, N., Liu, P. F., Ran, L., Xu, W. Y., Chen, J., Liang, Z., Liang, S., Huang, M. Y., Ma, X. C., Zhang, Q., Quan, J. N., Yan, P., Henning, S., Mildenberger, K., Sommerhage, E., Schäfer, M., Stratmann, F., and Wiedensohler, A.: Size-resolved and bulk activation properties of aerosols in the North China Plain, Atmos. Chem. Phys., 11, 3835–3846, doi:10.5194/acp-11-3835-2011, 2011. 1626

Gysel, M. and Stratmann, F.: WP3 – NA3: In-situ chemical, physical and optical properties of aerosols, Deliverable D3.11: Standardized protocol for CCN measurements, Tech. rep., http://www.actris.net/Publications/ACTRISQualityStandards/tabid/11271/language/en-GB/Default.aspx, 2013. 1625, 1627, 1642

Harris, E., Sinha, B., van Pinxteren, D., Tilgner, A., Fomba, K. W., Schneider, J., Roth, A., Gnauk, T., Fahlbusch, B., Mertes, S., Lee, T., Collett, J., Foley, S., Borrmann, S., Hoppe, P., and Herrmann, H.: Enhanced role of transition metal ion catalysis during in-cloud oxidation of SO_2, Science, 340, 727–730, doi:10.1126/science.1230911, 2013. 1623, 1630

Harris, E., Sinha, B., Van Pinxteren, D., Schneider, J., Collett, J., Fahlbusch, B., Foley, S., Fomba, K. W., Gnauk, T., Lee, T., Mertes, S., Roth, A., Borrmann, S., Hoppe, P., and Her-

ACPD
14, 1617–1645, 2014

rmann, H.: In-cloud sulafte addition to single particles resolved with sulfur isotope analysis HCCT 2010, Atmos. Chem. Phys. Discuss., submitted, 2014. 1623, 1630
Herrmann, H., Wolke, R., Muller, K., Bruggemann, E., Gnauk, T., Barzaghi, P., Mertes, S., Lehmann, K., Massling, A., Birmili, W., Wiedensohler, A., Wierprecht, W., Acker, K., Jaeschke, W., Kramberger, H., Svrcina, B., Bachmann, K., Collett, J. L., Galgon, D., Schwirn, K., Nowak, A., van Pinxteren, D., Plewka, A., Chemnitzer, R., Rud, C., Hofmann, D., Tilgner, A., Diehl, K., Heinold, B., Hinneburg, D., Knoth, O., Sehili, A. M., Simmel, M., Wurzler, S., Majdik, Z., Mauersberger, G., and Muller, F.: FEBUKO and MODMEP: field measurements and modelling of aerosol and cloud multiphase processes, Atmos. Environ., 39, 4169–4183, doi:10.1016/j.atmosenv.2005.02.004, 2005. 1620
IPCC report 2013: Working Group I contribution to the AR5 on Climate Change 2013: the Physical Science Basis, Cambridge University Press, Cambridge, UK, New York, NY, USA, http://www.ipcc.ch/report/ar5/wg1, 2013. 1619
Jayne, J., Leard, D., Zhang, X., Davidovits, P., Smith, K., Kolb, C., and Worsnop, D.: Development of an aerosol mass spectrometer for size and composition analysis of submicron particles, Aerosol Sci. Tech., 33, 49–70, 2000.
Köhler, H.: The nucleus and the growth of hygroscopic droplets, T. Faraday Soc., 32, 1152–1161, 1936. 1621
Krämer, M., Twohy, C. H., Hermann, M., Afchine, A., Dhaniyala, S., and Korolev, A.: Aerosol and cloud particle sampling, in: Airborne Measurements for Environmental Research: Methods and Instruments, edited by: Wendisch, M. and Brenguier, J. L., John Wiley & Sons, New York, Chichester, Weinheim, Brisbane, Singapore, Toronto, 2013. 1619
Lehmann, K., Massling, A., Tilgner, A., Mertes, S., Galgon, D., and Wiedensohler, A.: Size-resolved soluble volume fractions of submicrometer particles in air masses of different character, Atmos. Environ., 39, 4257–4266, doi:10.1016/j.atmosenv.2005.02.011, 2005. 1620
Lohmann, U. and Feichter, J.: Global indirect aerosol effects: a review, Atmos. Chem. Phys., 5, 715–737, doi:10.5194/acp-5-715-2005, 2005. 1619
Mertes, S., Lehmann, K., Nowak, A., Massling, A., and Wiedensohler, A.: Link between aerosol hygroscopic growth and droplet activation observed for hill-capped clouds at connected flow conditions during FEBUKO, Atmos. Environ., 39, 4247–4256, doi:10.1016/j.atmosenv.2005.02.010, 2005a. 1620
Mertes, S., Galgon, D., Schwirn, K., Nowak, A., Lehmann, K., Massling, A., Wiedensohler, A., and Wieprecht, W.: Evolution of particle concentration and size distribution observed upwind,

ACPD
14, 1617–1645, 2014

inside and downwind hill cap clouds at connected flow conditions during FEBUKO, Atmos. Environ., 39, 4233–4245, doi:10.1016/j.atmosenv.2005.02.009, 2005b. 1621

Oakes, J. and Feldman, H.: Statistical power for nonequivalent pretest-posttest designs: the impact of Change-Score versus ANCOVA models, Evaluation Rev., 25, 3–28, doi:10.1177/0193841X0102500101, 2001. 1628

Petters, M. D. and Kreidenweis, S. M.: A single parameter representation of hygroscopic growth and cloud condensation nucleus activity, Atmos. Chem. Phys., 7, 1961–1971, doi:10.5194/acp-7-1961-2007, 2007. 1621, 1625

Pringle, K. J., Carslaw, K. S., Spracklen, D. V., Mann, G. M., and Chipperfield, M. P.: The relationship between aerosol and cloud drop number concentrations in a global aerosol microphysics model, Atmos. Chem. Phys., 9, 4131–4144, doi:10.5194/acp-9-4131-2009, 2009. 1621

R version 2.15.3 (2013-03-01) – "Security Blanket" The R Foundation for Statistical Computing, ISBN 3-900051-07-0, 2013. 1629

Roberts, G. C. and Nenes, A.: A continuous-flow streamwise thermal-gradient CCN chamber for atmospheric measurements, Aerosol Sci. Tech., 39, 206–221, 2005. 1623, 1624

Rose, D., Gunthe, S. S., Mikhailov, E., Frank, G. P., Dusek, U., Andreae, M. O., and Pöschl, U.: Calibration and measurement uncertainties of a continuous-flow cloud condensation nuclei counter (DMT-CCNc): CCN activation of ammonium sulfate and sodium chloride aerosol particles in theory and experiment, Atmos. Chem. Phys., 8, 1153–1179, doi:10.5194/acp-8-1153-2008, 2008. 1625, 1626

Roth, A., Schneider, J., Mertes, S., van Pinxteren, D., Herrmann, H., and Borrmann, S.: Observation of nitrate and sulfate increase in cloud residual particles sampled in orographic clouds by single particle mass spectrometry during HCCT2010, Atmos. Chem. Phys. Discuss., in preparation, 2014. 1631

Schneider, J., Mertes, S., van Pinxteren, D., Tilgner, A., Herrmann, H., and Borrmann, S.:: In situ mass spectrometric analysis of cloud residual composition in orographic clouds during HCCT2010: Evidence for uptake of nitric acid in cloud droplets, Atmos. Chem. Phys. Discuss.„ in preparation, 2014. 1631

Senn, S.: Change from baseline and analysis of covariance revisited, Stat. Med., 25, 4334–4344, doi:10.1002/sim.2682, 2006. 1629

Svenningsson, B., Hansson, H. C., Martinsson, B., Wiedensohler, A., Swietlicki, E., Cederfelt, S. I., Wendisch, M., Bower, K. N., Choularton, T. W., and Colvile, R. N.: Cloud droplet

ACPD
14, 1617–1645, 2014

nucleation scavenging in relation to the size and hygroscopic behaviour of aerosol particles, Atmos. Environ., 31, 2463–2475, 1997. 1620

Svenningsson, I. B., Hansson, H. C., Wiedensohler, A., Ogren, J. A., Noone, K. J., and Hallberg, A.: Hygroscopic growth of aerosol-particles in the Po Valley, Tellus B, 44, 556–569, 1992. 1620

Tilgner, A., Majdik, Z., Sehili, A. M., Simmel, M., Wolke, R., and Herrmann, H.: SPACCIM: simulations of the multiphase chemistry occurring in the FEBUKO hill cap cloud experiments, Atmos. Environ., 39, 4389–4401, doi:10.1016/j.atmosenv.2005.02.028, 2005. 1620

Tilgner, A., Schöne, Bräuer, L. P., van Pinxteren, D., Hoffmann, E., Birmili, W., Mertes, S., Otto, R., Merkel, M., Weinhold, K., Deneke, H., Spindler, G., Haunold, W., Engel, A., Wéber, A., Wiedensohler, A., and Herrmann, A.: Critical assessment of meteorological conditions and flow connectivity during HCCT 2010, Atmos. Chem. Phys., submitted, 2014. 1622

Tuch, T. M., Haudek, A., Müller, T., Nowak, A., Wex, H., and Wiedensohler, A.: Design and performance of an automatic regenerating adsorption aerosol dryer for continuous operation at monitoring sites, Atmos. Meas. Tech., 2, 417–422, doi:10.5194/amt-2-417-2009, 2009. 1622

Wex, H., Hennig, T., Salma, I., Ocskay, R., Kiselev, A., Henning, S., Massling, A., Wiedensohler, A., and Stratmann, F.: Hygroscopic growth and measured and modeled critical super-saturations of an atmospheric HULIS sample, Geophys. Res. Lett., 34, L02818, doi:10.1029/2006GL028260, 2007. 1621

Wiedensohler, A.: An approximation of the bipolar charge-distribution for particles in the submicron size range, J. Aerosol Sci., 19, 387–389, 1988. 1623, 1626

Wiedensohler, A., Birmili, W., Nowak, A., Sonntag, A., Weinhold, K., Merkel, M., Wehner, B., Tuch, T., Pfeifer, S., Fiebig, M., Fjäraa, A. M., Asmi, E., Sellegri, K., Depuy, R., Venzac, H., Villani, P., Laj, P., Aalto, P., Ogren, J. A., Swietlicki, E., Williams, P., Roldin, P., Quincey, P., Hüglin, C., Fierz-Schmidhauser, R., Gysel, M., Weingartner, E., Riccobono, F., Santos, S., Grüning, C., Faloon, K., Beddows, D., Harrison, R., Monahan, C., Jennings, S. G., O'Dowd, C. D., Marinoni, A., Horn, H.-G., Keck, L., Jiang, J., Scheckman, J., McMurry, P. H., Deng, Z., Zhao, C. S., Moerman, M., Henzing, B., de Leeuw, G., Löschau, G., and Bastian, S.: Mobility particle size spectrometers: harmonization of technical standards and data structure to facilitate high quality long-term observations of atmospheric particle number size distributions, Atmos. Meas. Tech., 5, 657–685, doi:10.5194/amt-5-657-2012, 2012. 1623, 1626

ACPD
14, 1617–1645, 2014

Wobrock, W., Schell, D., Maser, R., Jaeschke, W., Georgii, H. W., Wieprecht, W., Arends, B. G., Mols, J. J., Kos, G. P. A., Fuzzi, S., Facchini, M. C., Orsi, G., Berner, A., Solly, I., Kruisz, C., Svenningsson, I. B., Wiedensohler, A., Hansson, H. C., Ogren, J. A., Noone, K. J., Hallberg, A., Pahl, S., Schneider, T., Winkler, P., Winiwarter, W., Colvile, R. N., Choularton, T. W., Flossmann, A. I., and Borrmann, S.: The Kleiner-Feldberg cloud experiment 1990 – an overview, J. Atmos. Chem., 19, 3–35, doi:10.1007/bf00696581, 1994. 1620

Wu, Z. J., Poulain, L., Henning, S., Dieckmann, K., Birmili, W., Merkel, M., van Pinxteren, D., Spindler, G., Müller, K., Stratmann, F., Herrmann, H., and Wiedensohler, A.: Relating particle hygroscopicity and CCN activity to chemical composition during the HCCT-2010 field campaign, Atmos. Chem. Phys., 13, 7983–7996, doi:10.5194/acp-13-7983-2013, 2013. 1630

ACPD
14, 1617–1645, 2014

Table 1. Overview of all defined Full Cloud Events (FCE) and Non Cloud Events (NE_NCE) for which CCN data are available at both valley stations.

	Start (CEST)	End (CEST)	LWC [$g m^{-3}$]	wd [°]	ws [$m s^{-1}$]
Cloud events					
FCE11.2	1 Oct 2010 20:50	2 Oct 2010 03:10	0.37	222.35	3.73
FCE11.3	2 Oct 2010 07:10	3 Oct 2010 00:30	0.35	223.98	6.58
FCE13.3	6 Oct 2010 06:50	7 Oct 2010 01:00	0.32	222.05	4.21
FCE22.0	19 Oct 2010 01:50	19 Oct 2010 09:00	0.29	226.76	5.96
FCE22.1	19 Oct 2010 21:10	20 Oct 2010 02:30	0.31	247.56	4.68
Non-cloud events					
NE_NCE0.1	7 Oct 2010 13:00	7 Oct 2010 18:50	–	49.40	1.27
NE_NCE0.2	8 Oct 2010 15:10	8 Oct 2010 18:30	–	59.70	2.24
NE_NCE0.3	9 Oct 2010 14:30	10 Oct 2010 09:30	–	68.88	4.67
NE_NCE0.4	10 Oct 2010 15:50	11 Oct 2010 03:30	–	51.36	5.66
NE_NCE0.5	11 Oct 2010 13:00	12 Oct 2010 04:40	–	51.61	5.72

ACPD
14, 1617–1645, 2014

Table 2. Mean critical diameter (D_c), standard deviation (σD_c) and hygroscopicity parameter κ, for Full Cloud Events (FCE: 11.2, 11.3, 13.3, 22.0 and 22.1) and Non Cloud Events (NE_NCE: 0.1, 0.2, 0.3, 0.4 and 0.5) at Goldlauter and Gehlberg station separated by supersaturation (SS). N gives the number of cases where measurements could be compared between Goldlauter and Gehlberg.

			upwind			downwind		
event	SS %	n	D_c nm	σD_c nm	κ^*	D_c nm	σD_c nm	κ
FCE	0.07	8	194.31	17.45	0.40	173.88	11.95	0.54
FCE	0.10	18	150.58	12.24	0.42	137.98	10.15	0.54
FCE	0.20	16	120.41	10.57	0.20	103.43	6.16	0.32
NCE	0.07	9	194.48	7.64	0.38	196.31	9.62	0.37
NCE	0.10	11	153.61	6.61	0.38	155.41	5.86	0.37
NCE	0.20	23	102.55	10.37	0.33	105.43	12.16	0.31
NCE	0.40	12	69.99	7.11	0.26	72.13	6.38	0.24

* Errors in κ are discussed in Sect. 3.2.

ACPD
14, 1617–1645, 2014

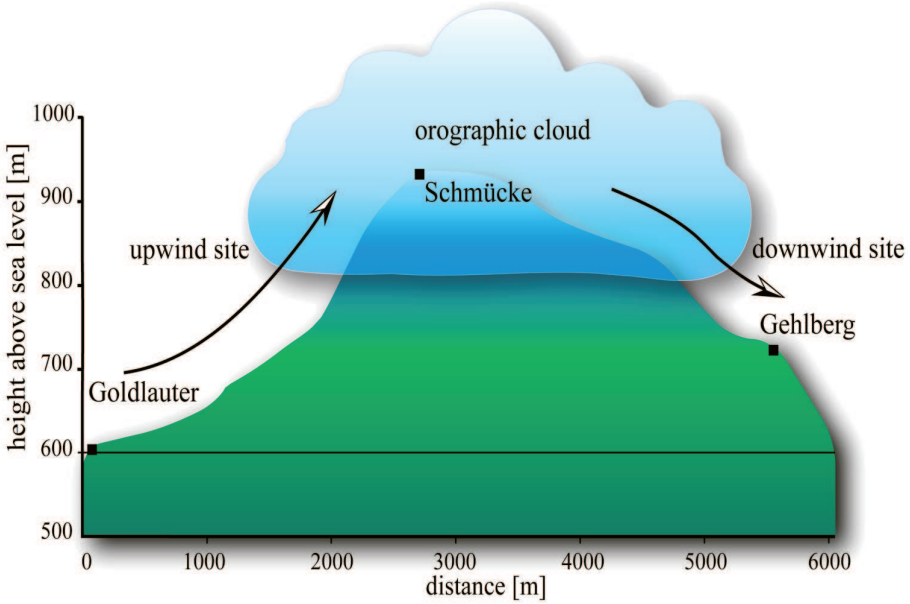

Fig. 1. Sketch of the terrain of the HCCT experiment. For an approaching flow from southwest, Goldlauter is the upwind station and Gehlberg the downwind station. This was the case for all defined full cloud events given in Table 1.

ACPD
14, 1617–1645, 2014

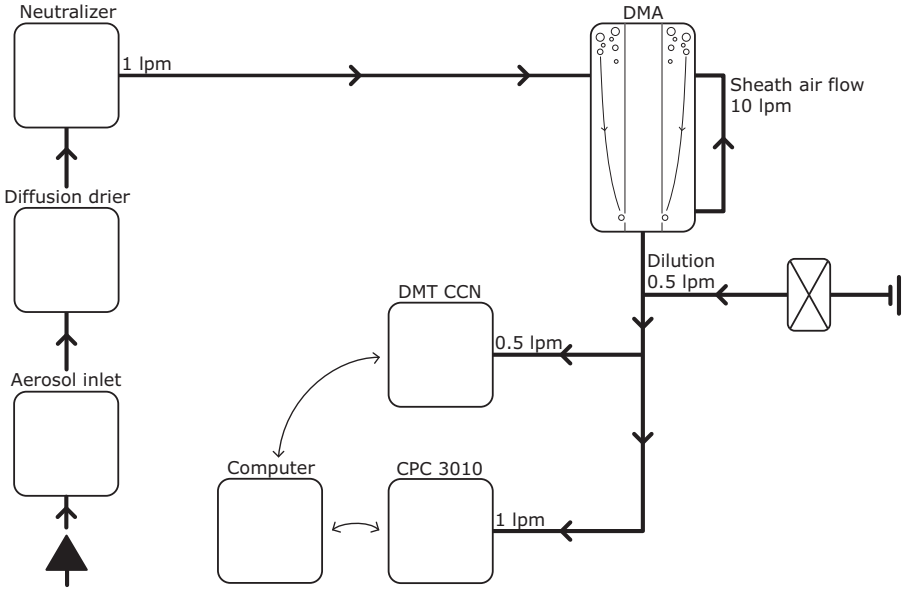

Fig. 2. Set-up for the size segregated CCN measurements. The experimental set-up was identical for the up- and downwind sites.

ACPD
14, 1617–1645, 2014

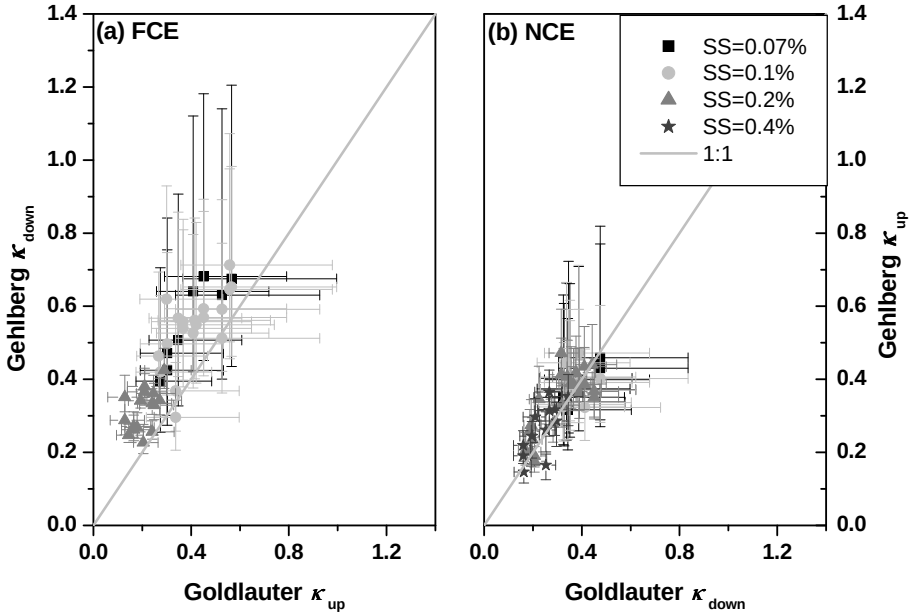

Fig. 3. Hygroscopicity parameter κ compared for up- and downwind stations during the Full Cloud Events (FCE, left panel) and during Non Cloud Events (NCE, right panel). The error bars represent a maximum absolute error in SS of ±0.02 % for SS ≤ 0.2 % and a 10 % relative uncertainty for SS > 0.2 % (Gysel and Stratmann, 2013).

ACPD
14, 1617–1645, 2014

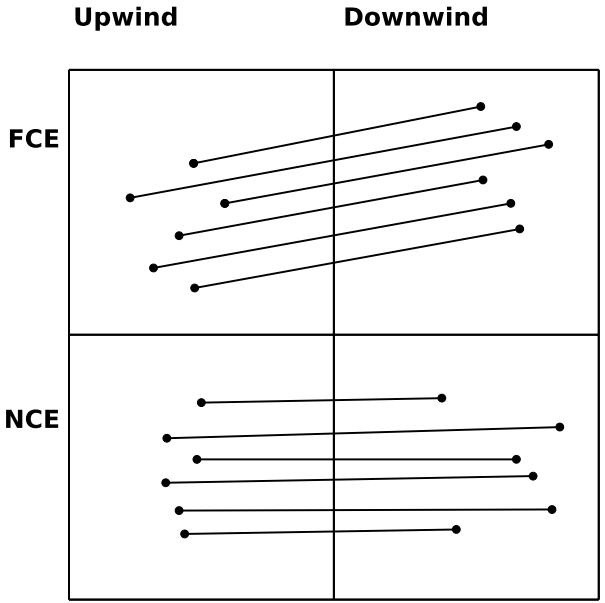

Fig. 4. Schematic depiction of the experimental mixed design. The starting and end points of the black lines refer to the critical diameter data points.

ACPD
14, 1617–1645, 2014

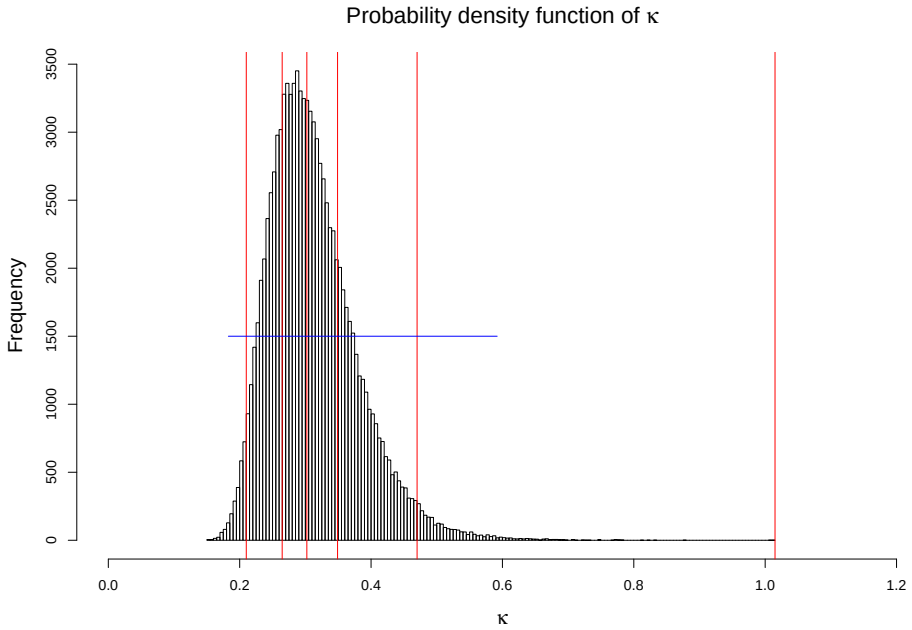

Fig. 5. The uncertainty distribution of one κ measurement, produced by 100 000 Monte Carlo samples. Red vertical lines from left to right depict the the 2.5, 25, 50, 75, 97.5 and 100th percentiles; blue horizontal line illustrates the range of the original error bars.

ACPD
14, 1617–1645, 2014

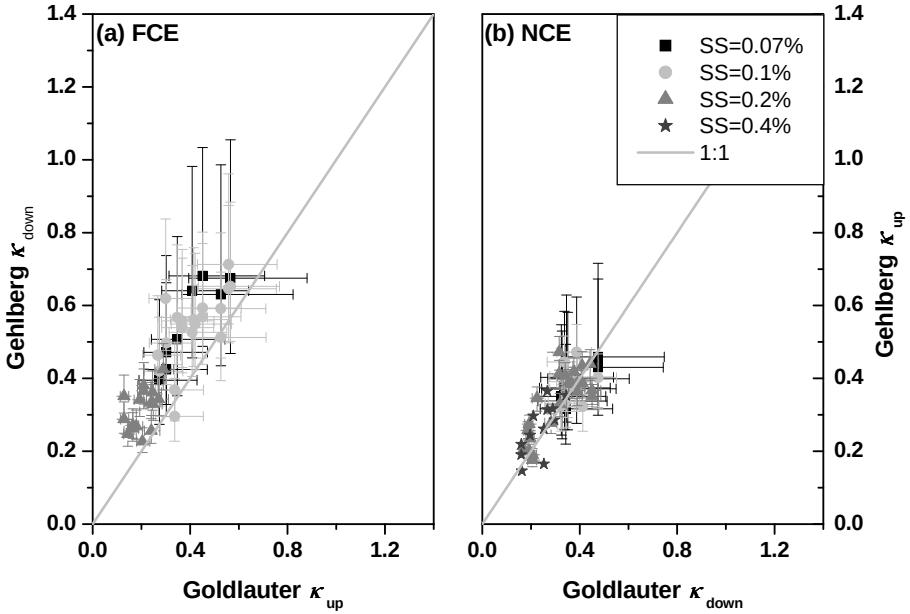

Fig. 6. Hygroscopicity parameter κ compared for up- and downwind station during the Full Cloud Events (FCE, left panel) and Non Cloud Events (NCE, right panel) as given in Fig. 3. However, the error bars are the 2.5 % and 97.5 % percentile limits for κ, produced by 100 000 Monte Carlo samples, representing a confidence level of 95 %.

ACPD
14, 1617–1645, 2014